Efficient water reduction by ruthenium-picolinate dye-sensitized photocatalyst under red light illumination

Taku Shimamura,[a] *Nobutaka Yoshimura,*[a] *Hiroki Otsuka,*[a†] *Masaki Yoshida,*[a‡] *Atsushi Kobayashi**[a]

[a]Department of Chemistry, Faculty of Science, Hokkaido University, North-10 West-8, Kita-ku, Sapporo 060-0810, Japan.

***Corresponding author's e-mail address**: akoba@sci.hokudai.ac.jp

[†]*Present address*: Department of Applied Chemistry, School of Engineering, The University of Tokyo, 7-3-1 Hongo, Bunkyo-ku, Tokyo 113-8656, Japan.

[‡]*Present address*: Department of Applied Chemistry for Environment, School of Biological and Environmental Sciences, Kwansei Gakuin University, 2-1 Gakuen, Sanda, Hyogo 669-1337, Japan.

KEYWORDS: Red light sensitizer, Ru(II) complex, Hydrogen production, Photocatalyst.

ABSTRACT: To utilize a wider region of the solar spectrum for solar-fuel production, we newly synthesized a heteroleptic Ru(II)-picolinate complex, $[Ru(H_4dpbpy)_2(pic)]^+$ (**Rupic**; H_4dpbpy = H_4dpbpy = 2,2′-bipyridine-4,4′-diphosphonic acid, Hpic = picolinic acid) as a red light-absorbing molecular photosensitizer. **Rupic** exhibited metal-to-ligand charge-transfer (MLCT) absorption and emission (λ_{abs} and λ_{em} = 491 and 711 nm, respectively) over a longer wavelength region than that observed with the bipyridine derivative $[Ru(H_4dpbpy)_2(bpy)]^{2+}$ (**Rubpy**, bpy = 2,2′-bipyridine). The Ru(III)/Ru(II) redox potential of **Rupic** (E_{ox} = +1.07 vs NHE) was approximately 0.27 V more negative than that of **Rubpy**, owing to the weaker ligand field strength of pic than that of bpy. Moreover, as expected, owing to the red-light absorption ability of **Rupic,** the photocatalytic H_2 evolution reaction activity of the **Rupic**-sensitized Pt-TiO_2 nanoparticles (apparent quantum yield, AQY ~3%) under red light illumination ($\lambda = 625 \pm 35$ nm) was significantly higher than that of its **Rubpy**-sensitized analog (AQY ~0.5%). These results indicate the superior photosensitizing performance of the Ru(II)-picolinate complex for H_2 production under sunlight illumination.

1. Introduction

Recently, molecular photosensitizers (PSs) have been attracting considerable attention because of their crucial role in solar energy conversion systems ranging from dye-sensitized solar cells (DSSCs) to artificial photosynthetic reactions including water splitting and CO_2 reduction.[1-9] One of the most widely used molecular PSs is the Ru(II)-trisbipyridyl complex $[Ru(bpy)_3]^{2+}$ (bpy = 2,2′-bipyridine), which exhibits strong visible absorption, at approximately 450 nm, originating from the metal-to-ligand charge transfer (MLCT) transition.[10-13] From the viewpoint of effective utilization of sunlight energy, extending the absorption band of a PS to cover the whole visible wavelength range is strongly required. The absorption ability of $[Ru(bpy)_3]^{2+}$ was limited to the wavelength range below 560 nm because of the strong ligand field afforded by the three bpy ligands; however, this limitation has been overcome by adjusting the field splitting and/or π-extension of the ligand.[10,11] In this regard, the most successful photosensitizers used in DSSCs are the Ru(II)-isothiocyanate complexes $[Ru(H_2dcbpy)_2(NCS)_2]$ and $[Ru(H_3tctpy)(NCS)_3]^-$, the so-called red and black dyes (H_2dcbpy = 2,2′-bipyridyl-4,4′-dicarboxylic acid, H_3tctpy = (2,2′:6′,6′′-terpyridyl-4,4′,4′′-tricarboxylic acid), respectively, which can almost absorb the full visible light range below 800 nm.[14-16] Unfortunately, however, these complexes are not suitable PSs for artificial synthesis such as water splitting because both the coordination bond with monodentate isothiocyanate ligands and carboxylate linkage are easily dissociated in highly polar solvents such as water.[17-20]

Replacing the isothiocyanate ligands of the red and black dyes with a chelating ligand of comparable ligand field strength is a well-established method to overcome the instability in the solution state. This is because of the larger stability constant and chelate ring closure in the *d–d*

excited state, which prevents the chelating ligand from being replaced by solvent molecules at the Ru center.[21] For example, Hanan et al. reported on the red light-driven photocatalytic H_2 evolution reaction using a tris-diimine complex, $[Ru(qpy)_3]^{2+}$ (qpy = 4,4′:2′,2″:4″,4‴-quaterpyridine), as the PS in the presence of $[Co(dmgH)_2]^{2+}$ as the molecular catalyst and triethanolamine as the sacrificial electron donor (SED).[22] Recently, Sakai and co-workers reported that trinuclear Ru(II) complex, $[Ru_3(dmbpy)_6(\mu\text{-HAT})]^{6+}$ (dmbpy=4,4′-dimethyl-2,2′-bipyridine, HAT=1,4,5,8,9,12-hexaazatriphenylene) acted as the near-infrared absorbing PS up to 800 nm for photocatalytic H_2 production in the presence of *L*-ascorbate SED.[23] Another simple example is the heteroleptic Ru(II) complex comprising a bidentate picolinate ligand $[Ru(bpy)_2(pic)]^+$ (Hpic = picolinic acid).[24-26] This complex shows red-shifted ^{1}MLCT absorption and ^{3}MLCT phosphorescence compared to those of $[Ru(bpy)_3]^{2+}$ and is stable in water even under visible light irradiation. Further, Tamaki et al. recently achieved photocatalytic CO_2 reduction under red light irradiation (λ >620 nm) using the dimethyl-functionalized derivative $[Ru(dmbpy)_2(pic)]^+$ as the PS in the presence of the Re(I) complex catalyst $[Re(dmbpy)(CO)_3Br]$ and the SED 1,3-dimethyl-2-phenyl-2,3-dihydro-1H-benzo[d]imidazole (BIH).[26] Although development of red light-absorbing Ru(II) PSs in homogeneous photocatalytic systems has been extended to supramolecular PSs and photocatalysts,[27-28] there has been little effort to utilize red light-absorbing Ru(II) PSs for heterogeneous nanoparticle photocatalysts in water reduction.[29-31]

In this study, we newly synthesized a phosphonate-functionalized derivative, $[Ru(H_4dpbpy)_2(pic)]^+$ (Figure 1; **Rupic**; H_4dpbpy = 2,2′-bipyridine-4,4′-diphosphonic acid), to develop a red light-absorbing and water-stable dye-sensitized photocatalyst for water reduction. Herein, we report on the synthesis and photophysical properties of the as-synthesized **Rupic** complex and discuss the photocatalytic H_2 evolution activity of a **Rupic**-sensitized Pt-TiO_2

nanoparticle photocatalyst (**Rupic**@Pt-TiO_2) in the presence of the SED *L*-ascorbate in aqueous solution. The phosphonate group was selected as the stable linker in water to immobilize Ru(II) complexes on the TiO_2 surface as reported in several literatures.[20,32,33] We found that **Rupic** exhibited a strong MLCT absorption band up to a wavelength of 640 nm and has a suitable photoredox potential to inject the photoexcited electron into TiO_2 and receive electrons from the electron donor, *L*-ascorbate. Further, **Rupic**@Pt-TiO_2 exhibited remarkably higher photocatalytic H_2 evolution activity than the bpy-derivative **Rubpy**@Pt-TiO_2 (**Rubpy** = $[Ru(H_4dpbpy)_2(bpy)]^{2+}$) under red light irradiation ($\lambda = 625 \pm 35$ nm).

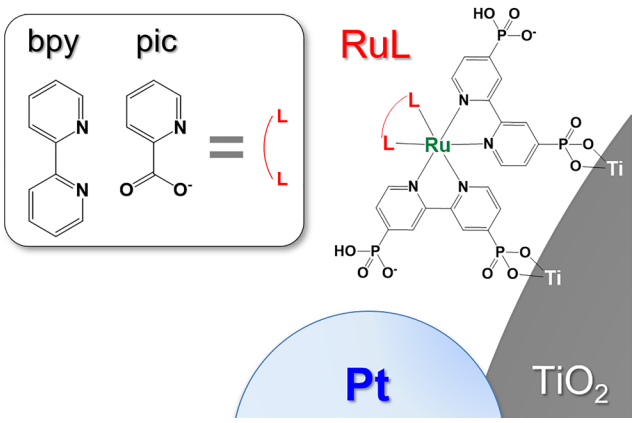

Figure 1. Schematic representation of the surface structure of the **RuL@Pt-TiO_2** nanoparticle (**L** = bpy or pic).

2. Material and Methods

2.1 Synthesis

All the commercially available starting materials were used as received without further purification. TiO_2 nanoparticles (SSP-M; ~15 nm diameter) were purchased from Sakai Chemical Industry Co., Ltd. The Pt cocatalyst-loaded TiO_2 nanoparticles were prepared using a previously reported photodeposition method.[34] The loading amount of the Pt cocatalyst was estimated to be 1.1 wt% by X-ray fluorescence spectroscopy. **Rubpy** and *cis*-$[Ru(H_4dpbpy)_2Cl_2]$ were synthesized using previously reported methods.[33,35] A Biotage Initiator$^+$ microwave synthesizer (Biotage Japan Ltd.) was used for the syntheses under microwave irradiation. Ultracentrifugation was conducted using a Himac CS120FNX ultracentrifuge (Eppendorf Himac Technologies Co. Ltd.).

2.1.1 Synthesis of $Et_3NH[Ru(H_3dpbpy)_2(2\text{-}pic)]$ (Rupic)

The starting materials, *cis*-$[Ru(H_4dpbpy)_2(bpy)_2Cl_2]$ (121.7 mg, 0.127 mmol, 1 eq), 2-pyridine carboxylic acid (26.3 mg, 0.213 mmol, 1.7 eq), ethanol (19.5 mL), and triethylamine (192 μL 1.37 mmol, 10.8 eq) were mixed in a 20 mL vial. The mixture was then stirred at 293 K for 5 min and then reacted at 150 °C for 15 min under microwave irradiation. Subsequently, excess acetone was added to the reaction solution to afford a reddish-brown solid. Yield: 99.8 mg (0.17 mmol, 74%). ^{1}H NMR (MeOD, 298 K): 8.80(m, 5H), 8.12(d, 2H), 7.94(m, 4H), 7.80(ddd, 1H,), 7.74(dd, 1H), 7.45(m, 1H), 3.18 (q, 6H), 1.30 (t, 9H). HRMS (MALDI-TOF) *m*/*z*: $[M - Et_3NH + 2H^+]^+$ Calcd for $C_{26}H_{24}N_5O_{14}P_4Ru_1$: 855.46. Found: 856.01. Anal. Calcd. (%) for $C_{26}H_{22}N_5O_{14}P_4Ru_1 \cdot (C_2H_5)_3NH \cdot 4H_2O$: C, 37.40; H, 4.51; N, 8.18. Found: C, 37.27; H, 4.41; N, 8.67.

2.1.2 Preparation of Ru(II) dye-sensitized Pt-TiO_2 nanoparticles

Rupic@Pt-TiO_2: Powdered Pt-TiO_2 nanoparticles (30 mg) were dispersed in a 1.25 mM aqueous solution of **Rupic** (6 mL) acidified by the addition of an HCl aqueous solution (pH 2.0). After sonication for 5 min, the mixture was stirred continuously overnight to immobilize **Rupic** onto the Pt-TiO_2 surface. The obtained **Rupic**-immobilized Pt-TiO_2 nanoparticles (**Rupic**@Pt-TiO_2) were collected by ultracentrifugation (50,000 rpm; 15 min) after which the supernatant solution was removed. After washing twice with an aqueous HCl solution (pH 2.0), the **Rupic**@Pt-TiO_2 sample was dried in vacuo at 298 K for 1 d.

Rubpy@Pt-TiO_2: Powdered Pt-TiO_2 nanoparticles (30 mg) were dispersed in a 1.25 mM aqueous solution of **Rubpy** (6 mL). After sonication for 5 min, 50 μL of a 60% $HClO_4$ aqueous solution was added, and the mixture was stirred continuously overnight to immobilize **Rubpy** on the Pt-TiO_2 surface. The obtained **Rubpy**-immobilized Pt-TiO_2 nanoparticles (**Rubpy**@Pt-TiO_2) were collected by ultracentrifugation (50,000 rpm, 15 min), after which the supernatant solution was removed. After washing twice with a 0.1 M $HClO_4$ aqueous solution, **Rubpy**@Pt-TiO_2 was dried in vacuo at 298 K for 1 d.

The amount of each Ru(II) dye immobilized on the Pt-TiO_2 nanoparticle surface was estimated by X-ray fluorescence and UV-vis absorption spectroscopy of the supernatant solution (see the Supporting Information).

2.2 Measurements

^{1}H NMR spectra were recorded on a JEOL ECZ-400S instrument. Elemental analysis was conducted at the analysis center of Hokkaido University. MALDI-TOF MS measurements were

carried out using a Bruker Autoflex Speed instrument with α-cyano-4-hydroxycinnamic acid as the matrix. Energy-dispersive XRF spectra were recorded using a Bruker S2 PUMA analyzer. Dynamic light scattering (DLS) analysis was performed using an OTSUKA ELSZ-1000SCI analyzer. UV-vis absorption and luminescence spectra were recorded on a Hitachi U-3000 spectrophotometer and JASCO FP-6600 spectrofluorometer, respectively; quartz cells with a 1-cm optical path length were used for both spectroscopic analyses. Prior to luminescence measurements, the sample solutions were degassed by N_2 bubbling for 20 min. Emission quantum yields (Φ_{em}) were measured using a Hamamatsu C9920-02 absolute photoluminescence quantum yield measurement system equipped with an integrating sphere apparatus and a 150-W continuous-wave Xe light source. Emission lifetime measurements were conducted using a Hamamatsu Photonics C4334 system equipped with a streak camera as the photodetector and nitrogen laser as the excitation light source (λ_{ex} = 337 nm). Cyclic voltammetry (CV) was performed using a HOKUTO DENKO HZ-3000 electrochemical measurement system equipped with a glassy carbon, Pt wire and Ag/AgCl electrodes as the working, counter and reference electrodes, respectively. Aqueous solution adjusted with pH 4.0 acetate buffer containing 0.1 M sodium perchlorate ($NaClO_4$) as the supporting electrolyte was deaerated by N_2 bubbling for 20 min and subsequently used in the CV experiments.

2.3 Photocatalytic H_2 evolution reactions

Under dark conditions, an *L*-ascorbic acid aqueous solution (0.02 M, pH 4.0) containing a Ru(II)-photosensitizer (100 μM Ru(II) complex) was placed into a homemade Schlenk flask-equipped quartz cell (volume = 255 mL) with a small magnetic stirring bar. Each sample flask was doubly sealed with a rubber septum. The mixed solution was deoxygenated by bubbling with Ar for 1 h. The flask was then irradiated from the bottom with blue (λ = 470 ± 10 nm, 70

mW), red (λ = 625 ± 25 nm, 53 mW) LED lamps (Opto-Device Lab. Ltd., OP6-4710HP2 and OP6-6310HP2, respectively) or Xe lamp (λ = 420-740 nm, 70 mW, Asahi Spectra Co., MAX-303). The temperature was controlled at 293 K using a custom-made Al water-cooling jacket with a water-circulating temperature controller (EYELA CCA-1111). Gas samples (0.6 mL) for each analysis were collected from the headspace using a gastight syringe (Valco Instruments Co. Inc.). The amount of evolved H_2 was determined using gas chromatography (Agilent 490 Micro Gas Chromatograph). The turnover number (TON) and turnover frequency (TOF) were estimated from the amount of evolved H_2, which required two photoredox cycles of the Ru(II)-photosensitizer to reduce one water molecule. The apparent quantum yield (AQY) was calculated using the following equation:

$$\mathrm{AQY} = N_e / N_p = 2N_{H2}/N_p \qquad \text{(eq. 1)}$$

where N_e, N_{H2}, and N_p are the numbers of reacted electrons, evolved H_2 molecules, and incident photons, respectively. When calculating the AQY, the wavelengths of all irradiated photons were assumed to be 470 and 625 nm for blue and red light, respectively.

2.4 Theoretical calculations

A density functional theory (DFT) calculation for **Rupic** was performed using the Gaussian 09 software package.[36] Geometry optimization was performed in the ground state using the B3LYP functional.[37,38] LANL2DZ effective core potentials and associated basis set were used.[39-41] The Cartesian coordinate of the geometrically optimized **Rupic** is shown in the supporting information. Visual representation of the molecular orbitals was obtained using GaussView 5.0.[42]

3. Results and Discussion

3.1 Photoelectrochemical properties

Figure 2 shows the UV-vis absorption and emission spectra of the **Rupic** and **Rubpy** complexes in aqueous solution at 298 K, while Table 1 summarizes the photophysical and electrochemical properties of these two complexes. **Rubpy**, which comprises three bpy-type ligands, presented similar absorption and emission spectra to those reported for the simple $[Ru(bpy)_3]^{2+}$ complex,[33,35] with π–π* and ^{1}MLCT absorption and ^{3}MLCT emission bands at 288, 460, and 643 nm, respectively. **Rupic** exhibited similar absorption and emission spectra to those of **Rubpy**, with, however, a notable difference in the MLCT transition. Specifically, the ^{1}MLCT absorption and ^{3}MLCT emission bands of **Rupic** (491 and 711 nm) were located at a significantly longer wavelength region than those of **Rubpy**. Notably, the lower ^{3}MLCT emission band of **Rupic** (approximately 85 nm lower than that of **Rubpy)** was also observed in the MeOH/EtOH frozen glass state at 77 K (Figure S1). This red shift of the MLCT transition induced by the introduction of the pic ligand is already discussed in the literature[24] through the comparison of $[Ru(bpy)_2(pic)]^+$ and $[Ru(bpy)_3]^{2+}$ without a phosphonate group. Briefly, coordination of the pic ligand carboxylate group stabilizes the MLCT transition state by electron donation to the Ru^{3+} state, resulting in lower MLCT absorption and emission energies. This is supported by the electrochemical measurements (Figure S2), wherein the cyclic voltammogram of **Rupic** clearly showed a quasi-reversible redox wave assignable to the Ru^{3+}/Ru^{2+} couple at 1.07 V (vs NHE) that was negatively shifted by approximately 0.27 V compared to that of **Rubpy**. Specifically, this negative shift indicates that the Ru^{3+} state of **Rupic** is more stable than that of **Rubpy** because of the weaker ligand field splitting of the pic ligand. The ^{1}MLCT absorption band of **Rupic** was located at a longer (by ~8 nm) wavelength than that of $[Ru(bpy)_2(pic)]^+$. This was

attributed to the lower π* orbital of the dpbpy ligand, with its four electron withdrawing phosphonate groups, than that of the simple bpy ligand. Our DFT calculation suggests that the highest-occupied molecular orbital (HOMO) distributes not only on the 4d orbital of Ru center but also the π orbital of carboxy group of pic ligand, while the lowest-unoccupied molecular orbital (LUMO) consists of π* orbital of dpbpy ligand (Figure S3). This result suggests that the lowest energy transition observed at around 500 nm should be the ^{1}MLCT transition from the Ru center to dpbpy ligand with the slight contribution of ligand-to-ligand (pic-to-dpbpy) charge transfer character.

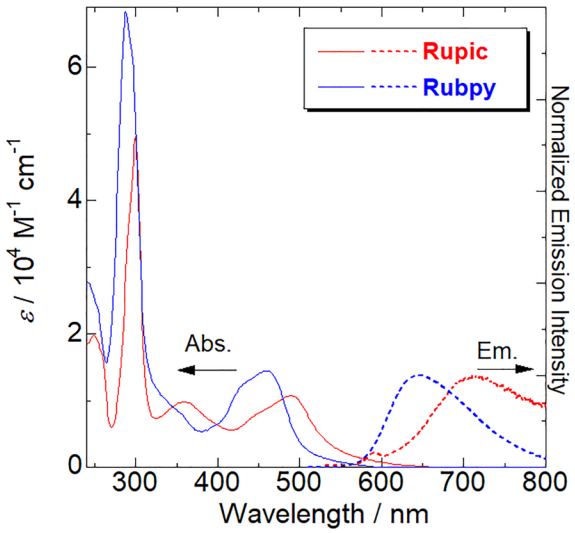

Figure 2. UV-vis absorption (solid lines) and emission (dotted lines) spectra of **Rupic** (red) and **Rubpy** (blue) measured in aqueous solution; λ_{ex} = 490 and 470 nm for **Rupic** and **Rubpy**, respectively.

Table 1. Photophysical and electrochemical data of **Rubpy** and **Rupic** in aqueous solution.

Complex	λ_{abs} / nm	$\lambda_{em,RT}$ [a] / nm	$\lambda_{em,77K}$ [a] / nm	τ_{em} [b] / ns	Φ [c]	k_r [d] / s^{-1}	k_{nr} [e] / s^{-1}	E_{ox} [f] / V vs NHE	E^*_{ox} [g] / V vs NHE
Rubpy	288, 460	643	597	483	0.05	1.0×10^5	2.0×10^6	+1.34	–0.73
Rupic	300, 491	711	682	68	0.01	1.5×10^5	1.5×10^7	+1.07	–0.75

[a] Emission maximum; [b] emission lifetime; [c] photoluminescence quantum yield. [d] Radiative rate constants (k_r) were estimated from the equation $k_r = \Phi/\tau_{em.}$ [e] Non-radiative rate constants (k_{nr}) were estimated from the equation $k_{nr} = k_r(1-\Phi)/\Phi$. [f] Estimated by CV measurement (Figure S2). [g] E^*_{ox} was estimated using the equation $E^*_{ox} = E_{ox} - E_{00}$, where E_{00} was approximated as $\lambda_{em,77K}$.

The emission decay and quantum yield of both complexes in aqueous solution were next evaluated (Table 1). Although the emission lifetime and quantum yield of **Rupic** (τ_{em} =68 nm, Φ = 0.01) were significantly lower than those of **Rubpy** (τ_{em} =483 nm, Φ = 0.05; Figure S4), the radiative rate constant (k_r) based on these results was comparable in the 10^5 s^{-1} range. Thus, the emission origins of both complexes could be assigned to the same ^{3}MLCT phosphorescence. The shorter lifetime and lower quantum yield of **Rupic** should originate from its approximately 10-fold larger non-radiative rate constant (k_{nr}) compared to that of **Rubpy**. This difference is reasonable from the viewpoint of the energy gap law, and the less steric pic ligand of **Rupic** may contribute to its higher k_{nr} value. This is also supported by DFT calculation (Figure S3); the HOMO of **Rupic** distributes to the carboxy group of pic ligand that may promote the vibrational relaxation from ^{3}MLCT transition state through solvent water molecules. The redox potential in the ^{3}MLCT excited state (E_{ox}*) was estimated based on the ^{3}MLCT phosphorescence energy (λ_{em}) at 77 K and the Ru^{3+}/Ru^{2+} redox potential in the ground state (E_{ox}). Although the E_{ox} of **Rupic** was more negative than that of **Rubpy** because of the weaker ligand field splitting of the

pic ligand, the estimated E_{ox}* for both complexes are comparable at approximately –0.7 V vs NHE, owing to the lower ^{3}MLCT emission energy of **Rupic** compared to that of **Rubpy**. The E_{ox}* values of both **Rupic** and **Rubpy** are sufficiently negative to inject the photo-excited electron to the conduction band of TiO_2 (conduction band minimum, CBM = −0.40 V vs NHE at pH 4.0).[43] Considering that the electron injection from photoexcited Ru(II)* complexes to TiO_2 was reported to occur within 1 ns after photoexcitation[33] that is quite shorter than τ_{em} of both complexes (see Table 1), the electron injection efficiency of both complexes should be comparable.

3.2 Characterization of Ru(II)-sensitized Pt-TiO_2 nanoparticles

The Ru(II) dye-sensitized Pt-TiO_2 nanoparticles (**Rupic**@Pt-TiO_2 and **Rubpy**@Pt-TiO_2) were characterized using X-ray fluorescence and UV-vis diffuse reflectance spectroscopy (Figure 3). All the nanoparticles exhibited strong Ti Kα and Kβ radiation in addition to the Pt Lα and Lβ radiation derived from the TiO_2 nanoparticles and Pt cocatalyst, respectively. Ru Kα radiation was clearly observed at 19.2 keV for both **Rupic**@Pt-TiO_2 and **Rubpy**@Pt-TiO_2, indicating the successful immobilization of these two Ru(II) dyes on the TiO_2 nanoparticle surface. Moreover, the intensity of the Ru Kα radiation indicated that a comparable amount of Ru(II) dye was immobilized on the Pt-TiO_2 surface. Ru(II) dye immobilization was further confirmed by UV-vis diffuse reflectance spectroscopy (Figures 3b and 3c), whereby the **Rupic**@Pt-TiO_2 and **Rubpy**@Pt-TiO_2 nanoparticles in the solid state exhibited very similar spectra with a characteristic ^{1}MLCT absorption band similar to that of the dye in aqueous solution. The amount of immobilized dye was estimated from the UV-vis absorption spectra of the supernatant solutions obtained in the dye sensitization process (see Figure S5 in the Supporting Information).

From the spectral data, we estimated the immobilized amounts of **Rupic** and **Rubpy** per 1 mg of Pt-TiO_2 to be 142 and 121 nmol, respectively (Table 2). These values are almost comparable to those of a similar Ru(II) dye comprising only two phosphonate groups, $[Ru(bpy)_2(H_4dpbpy)]^{2+}$ (116 nmol), which fully covered the TiO_2 nanoparticle surface.[44] Particle size distributions and zeta potentials of these nanoparticles were evaluated using a dynamic light scattering (DLS) technique to reveal the effect of Ru(II) dye surface modification (Table 2). The average particle sizes of **Rupic**@Pt-TiO_2 and **Rubpy**@Pt-TiO_2 were of the same order (Figure S6), suggesting that the dispersibility of these nanoparticles in water was hardly affected by ligand replacement, from bpy to pic, of the immobilized Ru(II) dye. This is consistent with their zeta potentials, whereby both nanoparticles exhibited a large negative potential below −30 mV that originated from the surface-immobilized and negatively charged Ru(II) molecules by deprotonation of the phosphonic acid groups. The more negative zeta potential of **Rupic**@Pt-TiO_2 compared to that of **Rubpy**@Pt-TiO_2 could be ascribed to the larger negative molecular charge of **Rupic**, which comprises a monoanionic pic ligand.

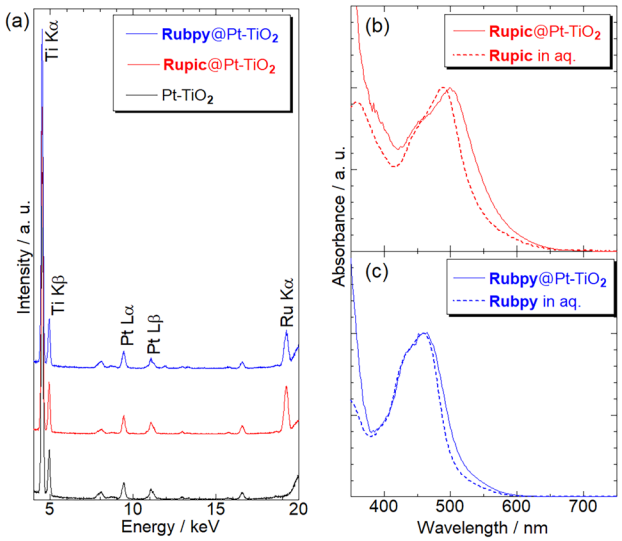

Figure 3. (a) XRF spectra of Pt-TiO_2 (black), **Rupic**@Pt-TiO_2 (red), and **Rubpy**@Pt-TiO_2 (blue) at 293 K. All spectra are normalized by the Ti Kα peak intensity. UV-vis diffuse reflectance spectra of (b) **Rupic**@Pt-TiO_2 and (c) **Rubpy**@Pt-TiO_2 in the solid state at 293 K. Dotted lines in panels (b) and (c) show the absorption spectra in aqueous solution.

Table 2. Characterization of **Rupic**@Pt-TiO_2 and **Rubpy**@Pt-TiO_2.

Photocatalyst	Amount of immobilized Ru(II) dye (nmol/1 mg TiO_2)[a]	Average particle size (nm)[b]	Zeta potential (mV)[b]
Rupic@Pt-TiO_2	119	367.4 ± 90.9	−41.99
Rubpy@Pt-TiO_2	94.6	276.1 ± 90.7	−30.24

[a] Estimated from the UV-vis absorption spectrum of the supernatant solution; [b] Estimated using the dynamic light scattering method in water.

3.3 Photocatalytic H_2 evolution

The photocatalytic H_2 evolution activities of the dye-sensitized photocatalysts, **Rupic**@Pt-TiO_2 and **Rubpy**@Pt-TiO_2, were evaluated in 20 mM *L*-ascorbic acid (H_2A) solution (pH 4.0, 0.5 M acetate buffer) under blue ($\lambda = 470 \pm 10$ nm, 70 mW cm^{-2}) and red ($\lambda = 625 \pm 35$ nm, 53 mW cm^{-2}) light irradiation and the results are shown in Figures 4(a) and 4(b), respectively. The estimated TOF per one Ru(II) photosensitizing dye and AQY for the first hour of reaction are listed in Table 3. Under blue light irradiation, both **Rupic**@Pt-TiO_2 and **Rubpy**@Pt-TiO_2 exhibited very high photocatalytic activities for H_2 evolution, and the turnover number per one Ru(II) photosensitizing dye (PS TON) for 3 h irradiation reached 400, which is the upper limit for consuming all the H_2A as the two-electron donor. The AQY value of **Rubpy**@Pt-TiO_2 was remarkably high (13.6%) even in a relatively dilute electron donor (20 mM), indicating the superior performance of this dye-sensitized photocatalyst. The TOF of **Rubpy**@Pt-TiO_2 was approximately 1.7-fold higher than that of **Rupic**@Pt-TiO_2. One plausible origin is the higher absorbance of **Rubpy** at 470 nm than that of **Rupic**. Indeed, the calculated absorbances at 470 nm based on the molar absorption coefficient of these dyes were 1.34 and 0.96, respectively, suggesting that 95.4% and 88.9% of the irradiated photons were absorbed by **Rubpy** and **Rupic**, respectively. The second plausible factor is the reactivity difference with the SED (Scheme 1), where the potential difference between the Ru^{3+}/Ru^{2+} couple of the Ru(II) dye and the oxidation potential of HA^- was estimated to be larger for **Rubpy** (0.63 V) than for **Rupic** (0.36 V), suggesting faster dye regeneration.[45] In fact, the emission quenching experiment using H_2A in aqueous solution revealed that the ^{3}MLCT emission of **Rubpy** was more effectively quenched by H_2A than that of **Rupic** (Figure S7 and Table S2). In addition, the less negative zeta potential of **Rubpy**@Pt-TiO_2 compared to that of **Rupic**@Pt-TiO_2 could reduce the electrostatic repulsion

between the photocatalyst surface and negatively charged HA^- electron donor. On the other hand, the rate of electron injection from the photoexcited Ru(II)* dye to TiO_2 was expected to be comparable because both **Rupic** and **Rubpy** have the same four phosphonate linkers and show a comparable redox potential in the ^{3}MLCT excited state (E_{ox}*).

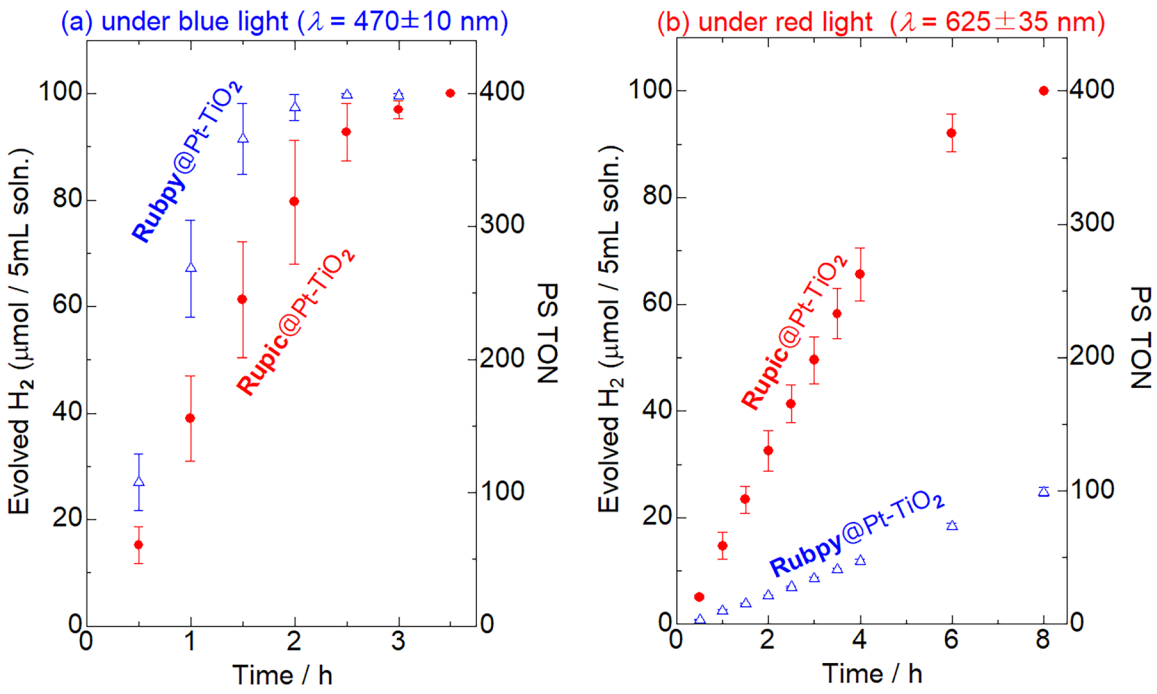

Figure 4. Photocatalytic H_2 evolution driven by **Rupic**@Pt-TiO_2 (red closed circles) and **Rubpy**@Pt-TiO_2 (blue open triangles) in a 20-mM *L*-ascorbic acid aqueous solution (100 μM of the Ru(II) complex in 0.5 M acetate buffer, pH 4.0) under (a) blue (λ_{ex}, 470 ± 10 nm) and (b) red (λ_{ex} = 625 ± 35 nm) light irradiation and Ar atmosphere.

Table 3. Results of the photocatalytic H_2 evolution in the presence of 20 mM *L*-ascorbic acid.

Photocatalyst	[**Ru**] (μM)	λ_{ex} (nm)	Abs. at λ_{ex}	TOF $(h^{-1})^a$	AQY $(\%)^b$
Rupic@Pt-TiO_2	100	470 ± 10	0.96	156	7.9
	100	625 ± 35	0.03	59	3.0
Rubpy@Pt-TiO_2	100	470 ± 10	1.34	258	13.6
	100	625 ± 35	< 0.01	12	0.5

[a] Turnover frequency and [b] apparent quantum yield for the first hour of reaction.

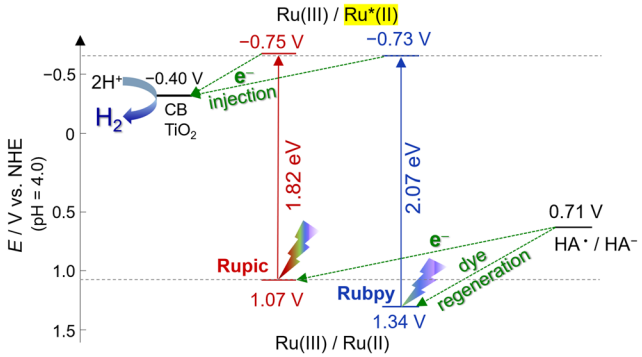

Scheme 1. Estimated energy diagrams of **Rupic**@Pt-TiO_2 (red) and **Rubpy**@Pt-TiO_2 (blue) in *L*-ascorbate (HA^-) aqueous solution (pH 4.0). The conduction band minimum of TiO_2 and oxidation potential of HA^- are reproduced from the literature.[43,45]

Contrasting results of the photocatalytic H_2 evolution were obtained under red light irradiation, as shown in Figure 4(b). After 8 h of reaction, the PS TON for **Rupic**@Pt-TiO_2 reached 400, indicating that all the H_2A was oxidized by the photocatalytic H_2 evolution reaction. This is further supported by the fact that the photocatalytic H_2 evolution reaction restarted following the

further addition of H_2A donor (Figure S8). In contrast, **Rubpy**@Pt-TiO_2 exhibited a PS TON of less than 100 even after 8 h of irradiation. The estimated TOF and AQY of **Rupic**@Pt-TiO_2 for the first hour of red light irradiation were approximately five times higher than those of **Rubpy**@Pt-TiO_2. This inverted order of photocatalytic activity under red light irradiation can be ascribed to the higher molar absorption coefficient of **Rupic** under red light. **Rupic**@Pt-TiO_2 exhibited a moderate ^{1}MLCT absorption band tail (ε = 972 and 324 M^{-1} cm^{-1} at 590 and 625 nm, respectively; Figure 3b), while negligible absorption was observed for **Rubpy**@Pt-TiO_2 (ε = 79 and 0 M^{-1} cm^{-1} at 590 and 625 nm, respectively; Figure 3c). This large difference in the red light absorption should overcome the smaller driving force of **Rupic**$^+$ dye regeneration by the H_2A donor compared to that of **Rubpy**, resulting in the higher photocatalytic activity of **Rupic**@Pt-TiO_2 under red light irradiation. In fact, these two photocatalysts exhibited almost comparable activity under wider range of visible light irradiation (λ = 420-740 nm, Figure S9), suggesting that the superior light absorption ability of **Rupic** than **Rubpy** can cancel out the smaller driving force for the electron donation from H_2 donor. Interestingly, the estimated AQY of **Rupic**@Pt-TiO_2 for the first hour of red light irradiation (~3%)[46] was comparable to that of a state-of-the-art heterogeneous H_2 evolution photocatalyst consisting of Pt-TiO_2 nanoparticles and a dibenzo-BODIPY-phenothiazine conjugate dye (AQY = 3.57% at 670 nm),[47] suggesting that the heteroleptic coordination structure of **Rupic** may contribute to the superior performance on the photo-induced charge-separation at the PS-TiO_2 interface.

4. Conclusions

In this work, we newly synthesized a red light-absorbing Ru(II)-picolinate photosensitizer with four phosphonate linkers, **Rupic**, and evaluated its photophysical and electrochemical properties by comparing them with the properties of its bipyridyl analog, **Rubpy**. The characteristic MLCT absorption and emission bands were red shifted by approximately 31 and 68 nm, respectively, in the solution state at 298 K by replacing the bpy ligand with pic, because of the weaker ligand field. Photophysical and electrochemical measurements revealed that the redox potentials of **Rupic** in the photoexcited and ground states (Ru(III)/Ru(II)* = –0.75 V and Ru(III)/Ru(II) = +1.07 V vs NHE) are sufficient to inject the photoexcited electron to TiO_2 and receive electrons from various electron donors such as *L*-ascorbate. The dye-sensitized photocatalyst **Rupic@Pt-TiO$_2$** stably produced H_2 in the presence of 20 mM L-ascorbate SED under blue- and red-light irradiation (λ =470 ± 10 and 625 ± 35 nm, respectively). The activity under red-light irradiation was estimated to be approximately five-fold higher photocatalytic H_2 evolution activity than its bipyridine analog, **Rubpy**@Pt-TiO_2, because of the effective red light absorption ability. Further development of **Rupic** derivatives and dye layering based on coordination bonding to cover the entire visible range is currently in progress.

Author Contributions

Conceptualization, A.K.; investigation, T.S.; resources, M.Y. and A.K.; methodology, H.O., M.Y. and A.K.; formal analysis and data curation, T.S., N.Y., and H.O.; writing—original draft preparation, T.S. and A.K.; writing—review and editing, M.Y. and A.K.; visualization, A.K.; supervision, A.K.; project administration, A.K.; funding acquisition, A.K. All authors have read and agreed to the published version of the manuscript.

ACKNOWLEDGMENT

The authors deeply thank Mr. T. Saito, D. Saito (Hokkaido University) and Prof. M. Kato (Kwansei Gakuin University) for their valuable discussion and support for the luminescence lifetime and quantum yield measurements. This study was supported by the ENEOS Hydrogen Trust Fund, Casio Science Promotion Foundation, Iwatani Naoji Foundation, JSPS KAKENHI, and Hokkaido University DX Doctoral Fellowship (grant numbers JP20H05082, JP22K19039, and JPMJSP2119).

REFERENCES

1. Youngblood, W. J.; Lee, S.-H. A.; Maeda, K.; Mallouk, T. E. Visible Light Water Splitting Using Dye-Sensitized Oxide Semiconductors, *Acc. Chem. Res.* **2009**, *42*, 1966–1973.

2. Ardo, S.; Meyer, G. J. Photodriven heterogeneous charge transfer with transition-metal compounds anchored to TiO_2 semiconductor surfaces, *Chem. Soc. Rev.* **2009**, *38*, 115–164.

3. Frischmann, P. D.; Mahata, K.; Würthner, F. Powering the future of molecular artificial photosynthesis with light-harvesting metallosupramolecular dye assemblies, *Chem. Soc. Rev.* **2013**, *42*, 1847–1870.

4. Ashford, D. L.; Gish, M. K.; Vannucci, A. K.; Brennaman, M. K.; Templeton, J. L.; Papanikolas, J. M.; Meyer, T. J. Molecular Chromophore−Catalyst Assemblies for Solar Fuel Applications, *Chem. Rev.* **2015**, *115*, 13006–13049.

5. Yamazaki, Y.; Takeda, H.; Ishitani, O. Photocatalytic reduction of CO_2 using metal complexes, *J. Photochem. Photobiol. C* **2015**, *25*, 106–137.

6. Zhang, X.; Peng, T.; Song, S. Recent advances in dye-sensitized semiconductor systems for photocatalytic hydrogen production, *J. Mater. Chem. A* **2016**, *4*, 2365–2402.

7. Gibson, E. A. Dye-sensitized photocathodes for H_2 evolution, *Chem. Soc. Rev.* **2017**, *46*, 6194–6209.

8. Dalle, K. E.; Warnan, J.; Leung, J. J.; Reuillard, B.; Karmel, I. S.; Reisner, E. Electro- and Solar-Driven Fuel Synthesis with First Row Transition Metal Complexes, *Chem. Rev.* **2019**, *119*, 2752–2875.

9. Kobayashi, A.; Takizawa, S.; Hirahara, M. Photofunctional molecular assembly for artificial photosynthesis: Beyond a simple dye sensitization strategy, *Coord. Chem. Rev.* **2022**, *467*, 214624.

10. Kalyanasundaram, K. Photophysics, photochemistry and solar energy conversion with tris(bipyridyl)ruthenium(II) and its analogues, *Coord. Chem. Rev.* **1982**, *46*, 159–244.

11. Juris, A.; Balzani, V.; Barigelletti, F.; Campagna, S.; Belser, P.; von Zelewsky, A. Ru(II) polypyridine complexes: photophysics, photochemistry, electrochemistry, and chemiluminescence, *Coord. Chem. Rev.* **1988**, *84*, 85–277.

12. Nicewicz, D. A.; MacMillan, D. W. C. Merging photoredox catalysis with organocatalysis: the direct asymmetric alkylation of aldehydes, *Science* **2008**, *322*, 77–80.

13. Yoon, T. P.; Ischay, M. A.; Du, J. Visible light photocatalysis as a greener approach to photochemical synthesis, *Nat. Chem.* **2010**, *2*, 527–532.

14. Nazeeruddin, M. K.; Kay, A.; Rodicio, I.; Humphry-Baker, R.; Mueller, E.; Liska, P.; Vlachopoulos, N.; Grätzel, M. Conversion of light to electricity by cis-X_2bis(2,2'-bipyridyl-4,4'-dicarboxylate)ruthenium(II) charge-transfer sensitizers (X = Cl^-, Br^-, I^-, CN^-, and SCN^-) on nanocrystalline titanium dioxide electrodes, *J. Am. Chem. Soc.* **1993**, *115*, 6382–6390.

15. Nazeeruddin, M. K.; Zakeeruddin, S. M.; Humphry-Baker, R.; Jirousek, M.; Liska, P.; Vlachopoulos, N.; Shklover, V.; Fischer, C.-H.; Grätzel, M. Acid-Base Equilibria of (2,2′-Bipyridyl-4,4′-dicarboxylic acid) Ruthenium(II) Complexes and the Effect of Protonation on Charge-Transfer Sensitization of Nanocrystalline Titania, *Inorg. Chem.* **1999**, *38*, 6298–6305.

16. Nazeeruddin, M. K.; Péchy, P.; Renouard, T.; Zakeeruddin, S. M.; Humphry-Baker, R.; Comte, P.; Liska, P.; Cevey, L.; Costa, E.; Shklover, V.; Spiccia, L.; Deacon G. B.; Bignozzi, C. A.; Grätzel, M. Engineering of Efficient Panchromatic Sensitizers for Nanocrystalline TiO_2-Based Solar Cells, *J. Am. Chem. Soc.* **2001**, *123*, 1613–1624.

17. Hoggard, P. E.; Porter, G. B. Photoanation of the tris(2,2'-bipyridine) ruthenium(II) cation by thiocyanate, *J. Am. Chem. Soc.* **1978**, *100*, 1457–1463.

18. Kohle, O.; Grätzel, M.; Meyer, A. F.; Meyer, T. B. The photovoltaic stability of bis(isothiocyanato)ruthenium(II)-bis-2,2'-bipyridine-4,4-dicarboxylic acid and related sensitizers, *Adv. Mater.* **1997**, *9*, 904–906.

19. Park, H.; Bae, E.; Lee, J.-J.; Park, J.; Choi, W. Effect of the anchoring Group in Ru-bipyridyl sensitizers on the photoelectrochemical behavior of dye-sensitized TiO_2 electrodes: carboxylate versus phosphonate linkages, *J. Phys. Chem. B* **2006**, *110*, 8740–8749.

20. Hanson, K.; Brennaman, M. K.; Luo, H.; Glasson, C. R. K.; Concepcion, J. J.; Song, W.; Meyer, T. J. Photostability of Phosphonate-Derivatized, Ru^{II} Polypyridyl Complexes on Metal Oxide Surfaces, *ACS Appl. Mater. Interfaces* **2012**, *4*, 1462–1469.

21. Durham, B.; Caspar, J. V.; Nagle, J. K.; Meyer, T. J. Photochemistry of tris(2,2′-bipyrdine)ruthenium(2+) ion, *J. Am. Chem. Soc.* **1982**, *104*, 4803–4810.

22. Rousset, E.; Chartrand, D.; Ciofini, I.; Marvaud, V.; Hanan, G. S. Red-light-driven photocatalytic hydrogen evolution using a ruthenium quaterpyridine complex, *Chem. Commun.* **2015**, *51*, 9261–9264.

23. Tsuji, Y.; Yamamoto, K.; Yamauchi, K.; Sakai, K. Near-Infrared Light-Driven Hydrogen Evolution from Water Using a Polypyridyl Triruthenium Photosensitizer, *Angew. Chem. Int. Ed.* **2018**, *57*, 208–212.

24. Norrby, T.; Börje, A.; Åkermark, B.; Hammarström, L.; Alsins, J.; Lashgari, K.; Norrestam, R.; Mårtensson, J.; Stenhagen, G. Synthesis, Structure, and Photophysical Properties of Novel Ruthenium(II) Carboxypyridine Type Complexes, *Inorg. Chem.* **1997**, *36*, 5850–5858.

25. Zhou, Q.; Zheng, Y.; Wang, X. Photoactivatable Ru complexes containing a Ru-O bond: Photoinduced ligand dissociation and DNA damage, *J. Photochem. Photobiol. A: Chem.* **2018**, *355*, 360–365.

26. Tamaki, Y.; Tokuda, K.; Yamazaki, Y.; Saito, D.; Ueda, Y.; Ishitani, O. Ruthenium picolinate complex as a redox photosensitizer with wide-band absorption, *Front. Chem.* **2019**, *7*, 327.

27. Zhang, L.-Y.; Yin, S.-Y.; Pan, M.; Liao, W.-M.; Zhang, J.-H.; Wang, H.-P.; Su, C.-Y. Binuclear Ru–Ru and Ir–Ru complexes for deep red emission and photocatalytic water reduction, *J. Mater. Chem. A* **2017**, *5*, 9807–9814.

28. Schott, O.; Pal, A. K.; Chartrand, D.; Hanan, G. S. A Bisamide Ruthenium Polypyridyl Complex as a Robust and Efficient Photosensitizer for Hydrogen Production, *ChemSusChem* **2017**, *10*, 4436–4441.

29. Swetha, T.; Mondal, I.; Bhanuprakash, K.; Pal, U.; Singh, S. P. First Study on Phosphonite-Coordinated Ruthenium Sensitizers for Efficient Photocatalytic Hydrogen Evolution, *ACS Appl. Mater. Interfaces* **2015**, *7*, 19635–19642.

30. Takijiri, K.; Morita, K.; Nakazono, T.; Sakai, K.; Ozawa, H. Highly stable chemisorption of dyes with pyridyl anchors over TiO_2: application in dye-sensitized photoelectrochemical water reduction in aqueous media, *Chem. Commun.* **2017**, *53*, 3042–3045.

31. Warnan, J.; Willkomm, J.; Ng, J. N.; Godin, R.; Prantl, S.; Durrant, J. R.; Reisner, E. Solar H_2 evolution in water with modified diketopyrrolopyrrole dyes immobilised on molecular Co and Ni catalyst–TiO_2 hybrids, *Chem. Sci.* **2017**, *8*, 3070-3079.

32. Raber, M. M.; Brady, M. D.; Troian-Gautier, L.; Dickenson, J. C.; Marquard, S. L.; Hyde, J. T.; Lopez, S. J.; Meyer, G. J.; Meyer, T. J.; Harrison, D. P. Fundamental Factors Impacting the Stability of Phosphonate-Derivatized Ruthenium Polypyridyl Sensitizers Adsorbed on Metal Oxide Surfaces, *ACS Appl. Mater. Interfaces* **2018**, *10*, 22821–22833.

33. Zigler, D. F.; Morseth, Z. A.; Wang, L.; Ashford, D. L.; Brennaman, M. K.; Grumstrup, E. M.; Brigham, E. C.; Gish, M. K.; Dillon, R. J.; Alibabaei, L.; Meyer, G. J.; Meyer, T. J.; Papanikolas, J. M. Disentangling the Physical Processes Responsible for the Kinetic Complexity in Interfacial Electron Transfer of Excited Ru(II) Polypyridyl Dyes on TiO_2, *J. Am. Chem. Soc.* **2016**, *138*, 4426−4438.

34. Park, H.; Choi, W.; Hoffmann, M. R. Effects of the preparation method of the ternary CdS/TiO_2/Pt hybrid photocatalysts on visible light-induced hydrogen production. *J. Mater. Chem.* **2008**, *18*, 2379–2385.

35. Norris, M. R.; Concepcion, J. J.; Glasson, C. R. K.; Fang, Z.; Lapides, A. M.; Ashford, D. L.; Templeton, J. L.; Meyer, T. J. Synthesis of Phosphonic Acid Derivatized Bipyridine Ligands and Their Ruthenium Complexes, *Inorg. Chem.* **2013**, *52*, 12492–12501.

36. *Gaussian 09*, Revision E.01, Frisch, M. J.; Trucks, G. W.; Schlegel, H. B.; Scuseria, G. E.; Robb, M. A.; Cheeseman, J. R.; Scalmani, G.; Barone, V.; Mennucci, B.; Petersson, G. A.; Nakatsuji, H.; Caricato, M.; Li, X.; Hratchian, H. P.; Izmaylov, A. F.; Bloino, J.; Zheng, G.; Sonnenberg, J. L.; Hada, M.; Ehara, M.; Toyota, K.; Fukuda, R.; Hasegawa, J.; Ishida, M.; Nakajima, T.; Honda, Y.; Kitao, O.; Nakai, H.; Vreven, T.; Montgomery, J. A., Jr.; Peralta, J. E.; Ogliaro, F.; Bearpark, M.; Heyd, J. J.; Brothers, E.; Kudin, K. N.; Staroverov, V. N.; Kobayashi, R.; Normand, J.; Raghavachari, K.; Rendell, A.; Burant, J. C.; Iyengar, S. S.; Tomasi, J.; Cossi, M.; Rega, N.; Millam, J. M.; Klene, M.; Knox, J. E.; Cross, J. B.; Bakken, V.; Adamo, C.; Jaramillo, J.; Gomperts, R.; Stratmann, R. E.; Yazyev, O.; Austin, A. J.; Cammi, R.; Pomelli, C.; Ochterski, J. W.; Martin, R. L.; Morokuma, K.; Zakrzewski, V. G.; Voth, G. A.; Salvador, P.; Dannenberg, J. J.; Dapprich, S.; Daniels, A. D.; Farkas, Ö.; Foresman, J. B.; Ortiz, J. V.; Cioslowski, J.; Fox, D. J. Gaussian, Inc., Wallingford CT, **2009**.

37. Becke, A. D. Density-Functional Thermochemistry. III. The Role of Exact Exchange, *J. Chem. Phys*. **1993**, *98*, 5648–5652.

38. Lee, C.; Yang, W.; Parr, R. G. Development of the Colle-Salvetti Correlation-Energy Formula into a Functional of the Electron Density, *Phys. Rev. B*, **1988**, *37*, 785–789.

39. Hay, P. J.; Wadt, W. R. Ab initio Effective Core Potentials for Molecular Calculations. Potentials for the Transition Metal Atoms Sc to Hg. *J. Chem. Phys*. **1985**, *82*, 270–283.

40. Wadt, W. R.; Hay, P. J. Ab initio Effective Core Potentials for Molecular Calculations. Potentials for Main Group Elements Na to Bi. *J. Chem. Phys*. **1985**, *82*, 284–298.

41. Hay, P. J.; Wadt, W. R. Ab initio Effective Core Potentials for Molecular Calculations. Potentials for K to Au Including the Outermost Core Orbitals. *J. Chem. Phys*. **1985**, *82*, 299–310.

42. *GaussView 5.0*: Dennington, R.; Keith, T.; Millam, J. Semichem Inc., Shawnee Mission, KS, **2009**.

43. Rothenberger, G.; Fitzmaurice, D.; Graetzel, M. Spectroscopy of Conduction Band Electrons in Transparent Metal Oxide Semiconductor Films: Optical Determination of the Flatband Potential of Colloidal Titanium Dioxide Films. *J. Phys. Chem.* **1992**, *96*, 5983−5986.

44. Furugori, S.; Kobayashi, A.; Watanabe, A.; Yoshida, M.; Kato, M. Impact of Photosensitizing Multilayered Structure on Ruthenium(II)-Dye-Sensitized TiO_2-Nanoparticle Photocatalysts, *ACS Omega* **2017**, *2*, 3901–3912.

45. Natali, M. Elucidating the Key Role of pH on Light-Driven Hydrogen Evolution by a Molecular Cobalt Catalyst. *ACS Catal.* **2017**, *7*, 1330−1339.

46. The AQY value for **Rupic**@Pt-TiO_2 under red light irradiation might have been overestimated because our reaction vessel was almost fully covered with Al foil, except for the bottom irradiation point, to prevent leakage of the irradiated light.

47. Suryani, O.; Higashino,Y.; Sato, H.; Kubo, Y. Visible-to-Near-Infrared Light-Driven Photocatalytic Hydrogen Production Using Dibenzo-BODIPY and Phenothiazine Conjugate as Organic Photosensitizer, *ACS Appl. Energy Mater.* **2019**, *2*, 448−458.

Graphical Abstract

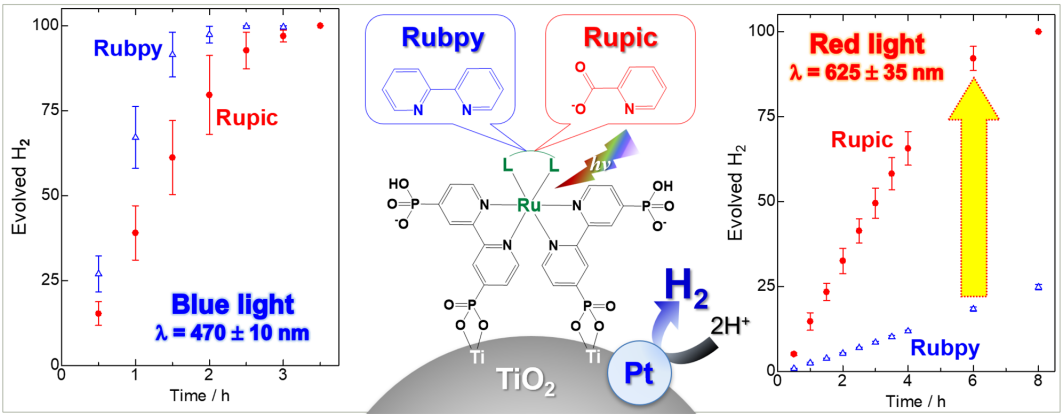

Highlights

- Ru(II)-picolinate photosensitizer bearing four phosphonate groups was synthesized
- Replacement of bipyridine with picolinate red-shifted the MLCT transition
- **Rupic**@Pt-TiO_2 showed higher activity than **Rubpy**@Pt-TiO_2 under red light irradiation